

# Size effect in steel-concrete bond: test results and modelling for smooth bars

D. Coronelli, P.G. Gambarova & P. Ravazzani  
Milan University of Technology, Milan, Italy

**ABSTRACT:** Size effects are studied here with reference to the bonding of smooth bars to both ordinary and high-performance concrete (NSC and HPC). To this purpose, 24 moderately-long anchorages ( $L/d_b = 10$ ), consisting of an artificially-roughened bar embedded in a concrete cylinder, were cast and tested up to the pull-out of the bars, which had 4 different diameters ( $d_b = 5, 12, 18$  and  $26$  mm). For each of the 8 cases examined here (4 diameters  $\times$  2 mixes), 3 nominally-identical specimens were tested. Furthermore, to have some information on the roles of specimen supports and bar roughness, 3 more specimens were cast and tested, bringing the specimen number to 27. Though the primary objective of this study is to investigate whether a general-type size-effect law applies to bond in high-performance silica-fume concrete, the modelling of an anchorage by means of a local elastic-fracturing-frictional bond-slip law is also carried out.

## 1 INTRODUCTION

Size effects in the structures made of quasi-brittle materials have been one of the most cherished topics in the last twenty years of the second millennium, and many experimental and theoretical studies have been carried out on a variety of plain-concrete and R/C structures, such as shear- and torsion-critical members, deep beams, slabs, fastenings and splices (Bazant and Chen, 1997; Ozbolt and Eligehausen, 1996).

On the basis of nonlinear fracture mechanics, crack cohesion and energy-balance considerations (between structural energy-release and concrete energy-consumption capacity), the well-known Bazant's size effect law (Fig.1) was formulated in the mid-Eighties, assuming a constant energy-supply per unit-surface of fracture, and similarity of the fracture shape and length. According to this law, size effects characterize the transition between the failure modes based on the achievement of a stress limit (yield criterion  $\Rightarrow$  ductile failures, no size effects) and those described by linear fracture mechanics ( $\Rightarrow$  brittle failures, maximum size effects).

Central to this transition is the energy dissipated at the fracture front, in the "fracture process zone", which is typical of cracking in heterogeneous, quasi brittle materials and structures (Shah and Ouyang, 1994; Bazant and Chen, 1997) and is the source of their softening behavior (and size effects).

As observed by Bazant and Chen (1997), "scaling

is the most important aspect of every physical theory". Consequently, scaling concerns also bar-concrete bond, even more since the bond stress-slip law of a smooth bar exhibits a strong softening. In such a case however, the bar-concrete interface should be considered as a sort of preoriented crack ("interfacial crack", length "a", Fig.2a, Stang et al., 1990), provided that "cracking" and "fracture process zone" are replaced with "debonding" and "transitional zone", the latter meaning that "hazy" part of the bonded interface, which is at the onset of slip and where bond is increasingly damaged, but still fairly efficient.

## 2 SIZE EFFECTS IN BOND

In spite of bond fundamental importance in R/C structures, limited attention has been devoted so far to size effects in bond. Two reasons may be quoted

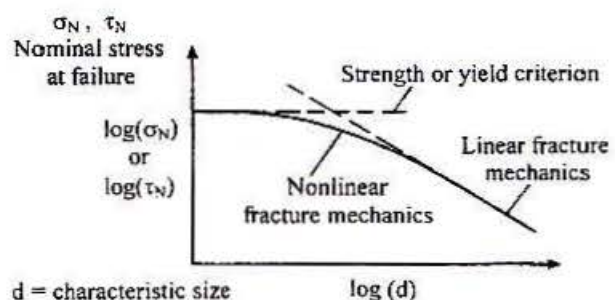


Fig.1 – Size effect law as observed in many concrete structures (Bazant and Desmorat, 1994).

with regard to this point: (a) the many parameters characterizing bond behavior and the ensuing scattering of the test results, which may overshadow size effects; and (b) the marked difference between the behaviors of the now rarely-used smooth bars and the commonly-used deformed bars.

Since the interface is more neatly defined in the former case, smooth bars have been investigated more extensively (Stang et al., 1990; de Larrard et al., 1993; Sener and Bazant, 1994; Bazant and Desmorat, 1994; Bazant et al., 1995; Lorrain and Hamouine, 1996), but deformed bars have been studied as well (Soroushian and Choi, 1989; de Larrard et al., 1993; Morita et al., 1994; Lorrain and Hamouine 1996; Elfegren et al., 1995; Esfahani and Rangan, 1998; Yerlici and Ozturan, 2000).

With reference to pull-out tests, a simplified model often adopted for debonding is depicted in Fig.2a, while some results on size effects in smooth and deformed bars are shown in Figs.2b,c. Finally, it is worth noting that many of the above-mentioned tests refer to ordinary concrete, and are not aimed specifically at size effects in bond.

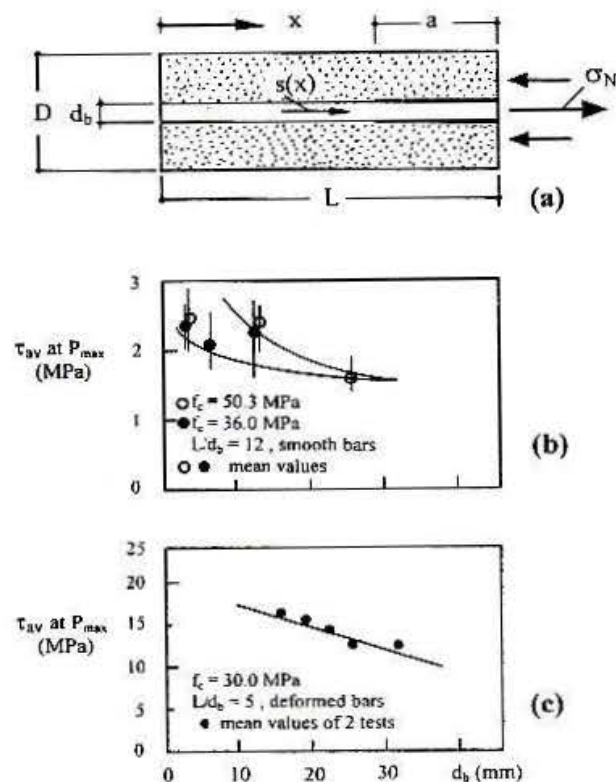


Fig.2 – (a) Debonding in a typical smooth-bar anchorage (Stang et al., 1990); (b) size effects in smooth bars (Bazant et al., 1995; see also Gambarova et al., 2000); and (c) size effects in deformed bars (Soroushian and Choi, 1989).

### 3 OBJECTIVE

This subproject is a part of a more ambitious project concerning the study of size effects in both smooth and high-bond (deformed) bars embedded in high-

performance concrete. The attention is here focused on smooth bars, anchored also in normal-strength concrete, for reference.

The primary objective is to investigate whether a general-type size-effect law can be established for anchorages in high-performance concrete, and to make comparisons with those embedded in normal-strength concrete.

## 4 EXPERIMENTAL PROGRAM

### 4.1 Specimen geometry

The general philosophy behind the design of the specimens - consisting of a single bar embedded in a concrete cylinder confined by a steel jacket (Fig.3) – was based on the two requirements of maximizing the expected size effects and avoiding the randomness of the “dishomogeneities”, which are typical of lightly-rusted smooth bars. The combination of these two requirements led to the choice of a moderately-long embedment length ( $L = 10 d_b$ , Fig.3), an artificially-roughened surface (see subsection 4.3), and a relatively-thick concrete cover ( $c = 4d_b$ , Fig.3).

As for the steel jacket (not necessary in well-enrobed smooth bars), its introduction was required in the case of deformed bars, in order to limit the extension of the possible splitting cracks. For this reason, the design of the jackets was based on the limitation of splitting to roughly 50% of the cover thickness, at the expected peak load. Once the jackets had been designed for high-bond bars, they were scaled-down for smooth bars, where they acted as formworks.

Four diameters were adopted (Fig.4): 3 values ( $d_b = 5, 12$  and  $26$  mm) were selected in such a way that the ratio between the bonded surfaces of two contiguous diameters was a constant ( $A_{26}/A_{12} \cong A_{12}/A_5 \cong 5$ ), while the 4<sup>th</sup> value ( $d_b = 18$  mm) represents commonly-used medium-size bars.

Specimen geometry was dictated by the requirement of perfect similitude (Fig.4), which was enforced also on the smallest details.

### 4.2 Materials

Two concrete mix-designs were studied, in order to prepare a normal-strength concrete ( $f_c = 29$  MPa at 28 days; cement content =  $300 \text{ kg/m}^3$ ; water/cement ratio = 0.65) and a high-performance concrete ( $f_c = 65$  MPa at 28 days;  $c = 400 \text{ kg/m}^3$ ; silica fume =  $40 \text{ kg/m}^3$ ;  $w/c+sf = 0.36$ ), the aggregate being mixed and with a maximum size of 12 mm. The strength of the latter mix had to take into account the necessity of preventing bar yielding before the full exploitation of bond, in the case of deformed bars.

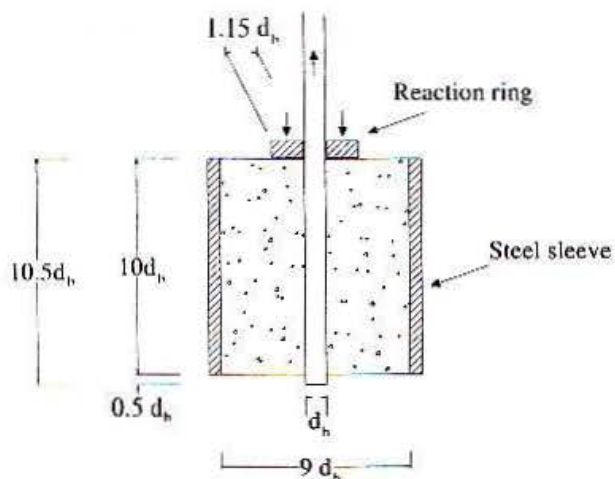


Fig.3 - Specimen geometry and reaction ring.

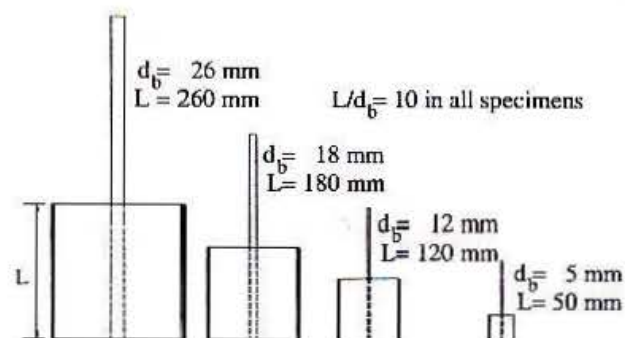


Fig.4 - Different sizes considered in this project:  $A_2/A_5 \cong 5$ .

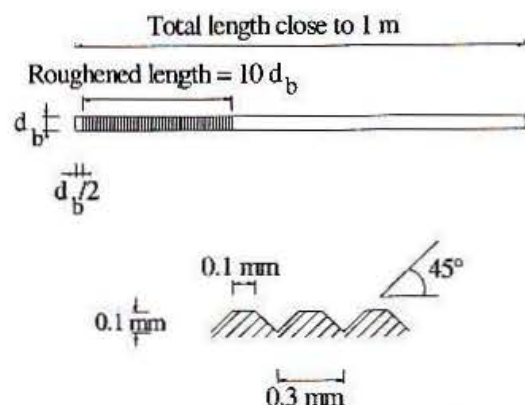


Fig.5 - Artificial roughness of bar surface, representing a heavily-corroded bar.

The bars were machined at the lathe, starting from commercial bars ( $f_y = 800-1000$  MPa).

In all, 27 specimens were tested, since for each of the 8 different cases examined here (4 diameters x 2 mixes), 3 nominally-equal specimens were cast (Table 1). For the preliminary checks on the loading procedure and on the instrumentation, 3 further specimens were prepared and tested (the details are given in the last subsection).

### 4.3 Surface conditions of the bars

In order to guarantee the uniformity of the surface, whatever the diameter may be, 24 bars were artificially-roughened at the lathe, as shown in Fig.5 ( $t = 100 \mu\text{m}$ ;  $s = 0.3$  mm;  $\alpha = 45^\circ$ ). Reference was made to heavily-pitted bars ( $t = 150-200 \mu\text{m}$ ;  $s = 2-2.5$  mm, see Rehm in Park and Paulay, 1978) and to lightly-rusted bars ( $t = 30-50 \mu\text{m}$ ;  $s = 1.5-2$  mm), while the bars "as rolled" are definitely smoother ( $t = 10-15 \mu\text{m}$ ;  $s = 1-1.5$  mm).

According to Fig.5, the depth of the pits ( $100 \mu\text{m}$ ) represents a moderate corrosion, but the spacing of the pits ( $0.3$  mm) makes the surface conditions much closer to heavy corrosion. This should be taken into account, when looking at the results of the pull-out tests!

Of course each bar was roughened only along the embedded length ( $L = 10d_b$ , Figs.4,5).

### 4.4 Instrumentation and test set-up

Measuring two displacements – at the loaded end and at the free end of the bar – was considered sufficient, given the relative simplicity of the tests. Three LVDTs were used, 2 at the loaded end (at  $180^\circ$ , Fig.6) and one at the free end. In both cases, the relative displacement (slip) was measured with respect to the undisturbed concrete.

The tests were displacement-controlled, and the feedback signal was sent to the control system of the press by the LVDT of the press, which measured the relative displacement of the heads.

At a displacement rate of  $5 \mu\text{m/s}$ , all specimens reached a maximum bar slip of  $9$  mm ( $\cong 1/3 d_{b,\text{max}}$ ).

Two electromechanical loading machines were used, but the smallest specimens ( $d_b = 5$  mm) were tested in an INSTRON press (capacity 100 kN), while for all the other specimens a bigger machine was necessary (Schenck press, capacity 1000 kN). In both cases the test set-ups were very similar (Ravazzani, 2001).

It is worth noting that also the reaction ring placed between the reaction plate and the specimen respected geometric similitude (Figs.3 and 6).

Finally, a few words should be devoted to the boundary conditions of the specimen. As already mentioned, in all specimens the ring shown in Fig.3 was used (outer diameter  $3.3d_b$ ).

However, to assess the effects of a concentrated restraint (= reaction ring), two extra specimens ( $d_b = 18$  mm) were cast and tested, the first with a reaction ring and the second with a reaction disk extended to the entire bottom section of the concrete cylinder.

Since the two load-slip curves were perfectly coincident ( $s \leq 1$  mm, Ravazzani, 2001), the worries about the possible effects of the reaction ring turned out to be groundless. In these specimens the reinforcement consisted of a deformed bar, the

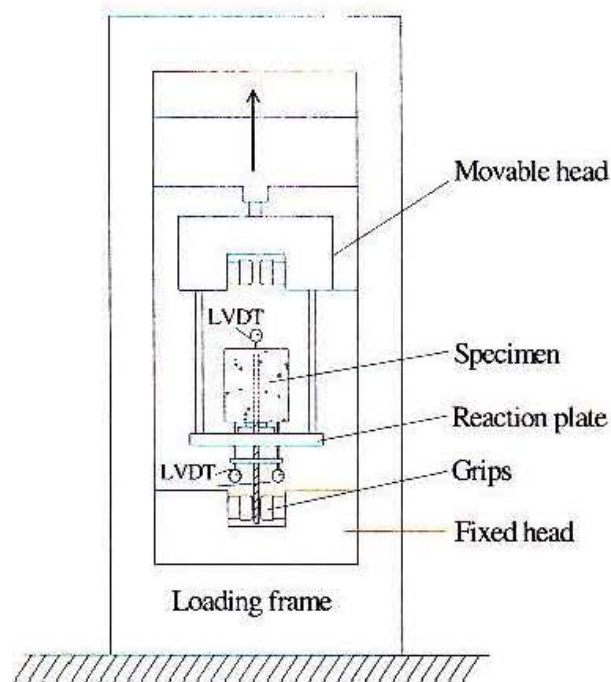


Fig.6 – Test set-up and instrumentation ( $d_b = 12, 18$  and  $26$  mm, Schenck press).

embedment length was shorter ( $L/d_b = 5.4$ ), and a high-strength concrete was used ( $f_c = 98$  MPa).

## 5 TEST RESULTS AND COMMENTS

As previously mentioned, the total number of the tests was 27, of which 24 were carried out to study size effects in bond (roughened bars), and 3 were “preliminary” tests (two on deformed bars, with different specimen supports, and one on a smooth bar “as rolled”).

All tests ran smoothly, even if the falling branch (past the peak load) was always very steep, slightly more in the HPC specimens and in those provided with small-diameter bars. However, the control of

the tests was never lost, and the slip at both ends of the bars was always recorded.

A summary of the test results is presented in Table 1, together with specimen designation and main geometric characteristics. In two cases (Specimens HS3-A and NS2-C), in spite of the regularity of the tests, the peak loads were so much lower than in the two companion tests, that the results were ignored.

### 5.1 Load-slip curves

Two typical response curves are shown in Fig.7, where the thick and thin lines refer to the loaded and unloaded ends respectively. In all HPC specimens full debonding is reached slightly before the attainment of the peak load, as shown by the displacements at the unloaded ends, which start at a load level always greater than 0.95 (Fig.7a). Only after a loaded-end slip equal to 1-4 mm ( $d_b = 5-26$  mm), the end displacements coincide, and bond resistance is ensured by the friction between two bodies, the bar and the concrete cylinder.

In all NSC specimens full debonding is reached practically at the very attainment of the peak load (Fig.7b), and after a much lower loaded-end slip (0.5 - 0.8 mm) the end displacements coincide.

However, in both HPC and NSC specimens the “tail” of the response curves was always decreasing with no clear asymptotes. One possible explanation may be found in the shrinkage-induced confinement exerted by the concrete on the bar: the larger the slip, the greater the damage at the interface and in the closest concrete layer, at the expense of the confinement (bond under variable confinement).

In order to quantify the favorable effects that the surface roughening has on bond, specimen NS3-P was reinforced with a smooth bar “as rolled”. Its load-slip curve is shown in Fig.7b. The comparison is amazing and need not be commented. The behavior of Specimen NS3-P seems to confirm the

Table 1 – Specimen designation and geometry, and summary of the test results:  $d_b$  = bar diameter;  $c$  = concrete cover;  $t$  = jacket thickness;  $L$  = embedment length;  $P_{max}$  = maximum load, or peak load;  $P_{res}$  = residual capacity;  $s(P_{max})$  = loaded-end slip at the maximum load. Specimen designation: N = NSC; H = HPC; S = smooth bar; D = deformed bar; 1,2,3,4  $\Rightarrow d_b = 5, 12, 18, 26$  mm; A,B,C  $\Rightarrow$  specimens tested in each case; P = preliminary test.

Concrete	Specimen	$d_b/c/L$ (mm)	$P_{max}$ (kN)	$[P_{res}/P_{max}]_{av}$	$[s(P_{max})/d_b]_{av}$
NSC - $f_c = 40$ MPa	NS3-P	18/72/4.0/180	16.3	31%	0.40%
HPC - $f_c = 98$ MPa	HD3-P-A/B	18/72/10.0/180	152/155 ( $s=1$ mm)	--	--
NSC $f_c = 29$ MPa	NS1-A/B/C	5/20/1.2/50	8.0/9.0/6.5	8%	2.96%
	NS2-A/B	12/48/3.0/120	29.8/31.7	12%	1.59%
	NS3-A/B/C	18/72/4.0/180	52.8/51.7/38.8	14%	1.23%
	NS4-A/B/C	26/104/6.0/260	66.8/51.4/36.7	14%	0.69%
HPC $f_c = 65$ MPa	HS1-A/B/C	5/20/3.0/50	11.5/13.3/12.5	20%	5.06%
	HS2-A/B/C	12/48/7.0/120	61.8/51.6/49.0	22%	2.83%
	HS3-B/C	18/72/10.0/180	112.6/111.0	25%	2.54%
	HS4-A/B/C	26/104/15.0/260	134.0/215.0/273.7	32%	1.83%

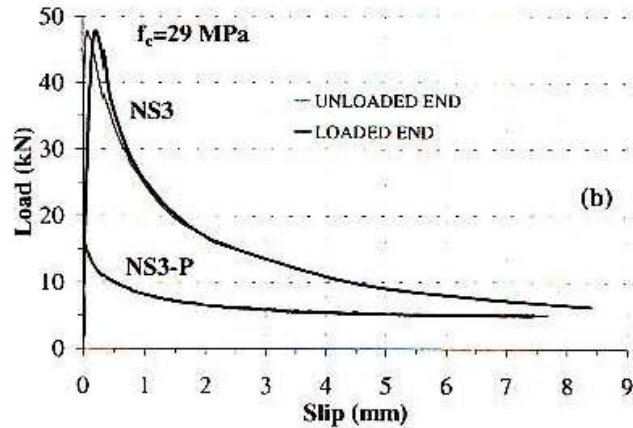
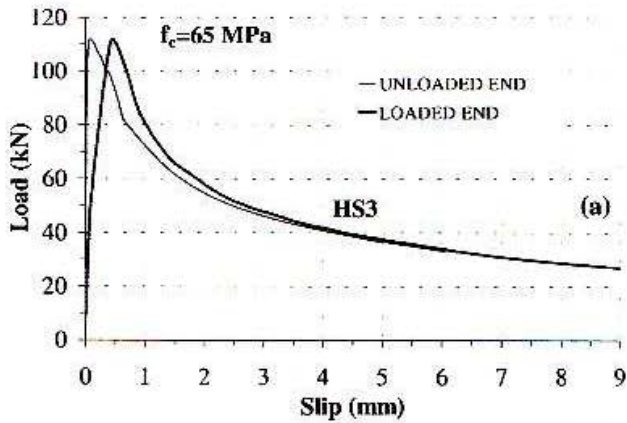


Fig. 7 – Typical load-slip curves ( $d_b = 18$  mm): (a) mean curves of Specimens HS3-A/B/C, high-performance concrete; and (b) mean curves of Specimens NS3-A/B/C, normal-strength concrete. “As-rolled surface” in Specimen NS3-P.

previous explanation, since a smoother surface is less damaging for the surrounding concrete and less detrimental to the confinement action; of course, friction is less efficient on the whole.

Fig.8 summarizes all the results, in terms of nominal bond strength (Fig.8a) and loaded-end slip (Fig.8b). Size effects are sizeable indeed!

It is worth noting that the scattering of the results is always very limited, except in the case of the largest bars in high-performance concrete ( $d_b = 26$  mm, see Table 1). This rather incomprehensible scattering led to the exclusion of the lowest values from any successive treatment.

In Fig.9 the plots of the average bond-stress/bar-slip curves, put in a dimensionless form, are strikingly similar, and their differences seem related more to the experimental scattering than to some other mechanical aspect. The only false note is represented by the smallest anchorage in normal-strength concrete ( $d_b = 5$  mm, Fig.9b), whose ascending branch is definitely very steep.

### 5.2 Size effects

As observed by Bazant et al. (1995), the post-peak softening exhibited by the load-displacement curves

is an indication of possible size effects, which may be described by the size-effect law earlier proposed by Bazant himself (see Eq.1), where the parameters to be measured are : the nominal strength of the anchorage  $\sigma_N = 4P_{max}/\pi d_b^2$ , and the residual nominal strength  $\sigma_o = 4P_{res}/\pi d_b^2$  (frictional strength):

$$\sigma_N - \sigma_o = B f [1 + (d_b/d_o)]^{1/2} \quad (1)$$

The ratio ( $d_b/d_o$ ) is the “relative size” and  $f$  is a strength parameter of the material, such as  $f_c$  or  $f_{ct}$ , which are equally suitable (in the following reference is made to  $f_c$ ).  $B$  and  $d_o$  are two constants, that have to be evaluated from the test data, by means of a regression procedure. Needless to say, the “characteristic size” of the problem coincides with  $d_b$  in our case.

The residual frictional strength was determined from the tails of the load-slip curves ( $s = 9$  mm), and its average values were  $\cong 127$  and  $\cong 26$  MPa (HPC and NSC respectively). However, contrary to the expectations there was a sizeable scattering among the 4 sets of specimens (+18/-10% with respect to the mean value, HPC). Generally speaking, the largest and/or lowest values were exhibited by the NSC specimens and by the largest diameters. On the

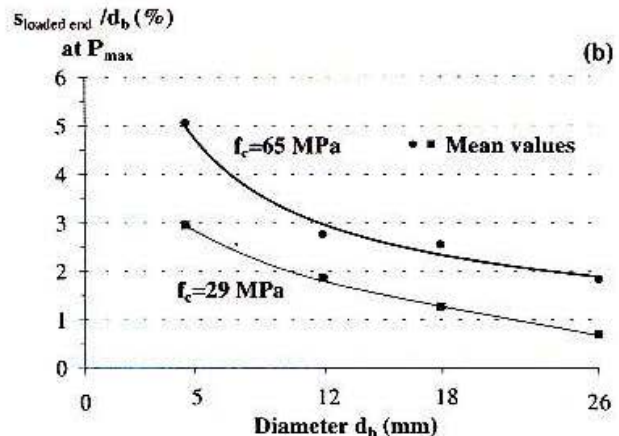
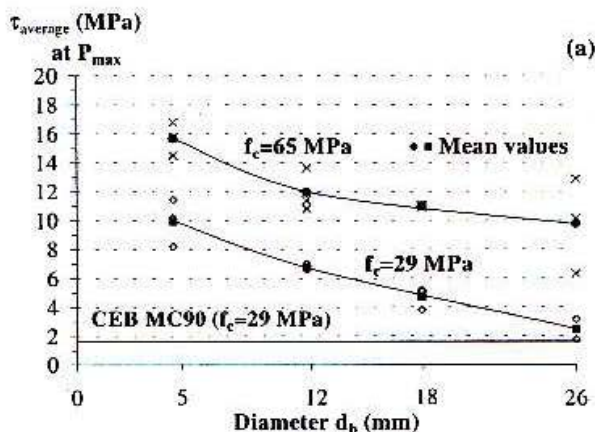


Fig.8 – Summary of the test results at maximum load (22 tests out of 24) : (a) average bond-stress, and (b) bar slip at the loaded end as a function of bar diameter.

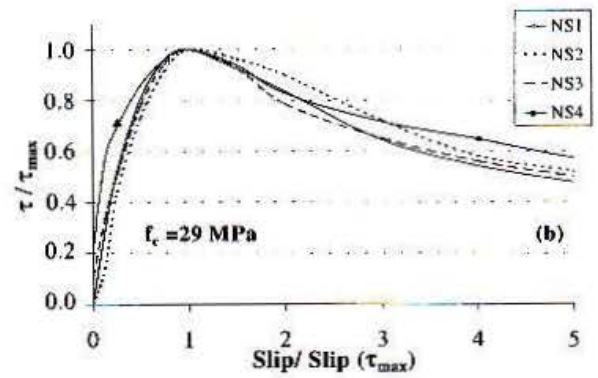
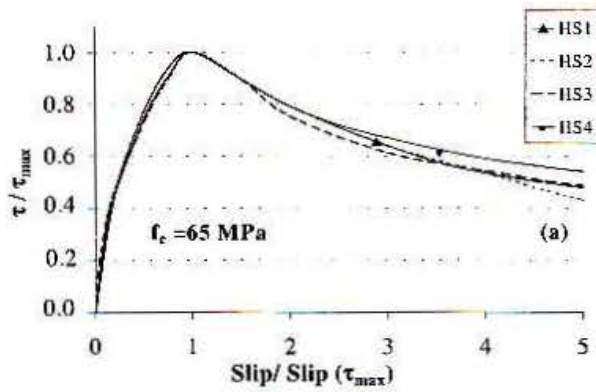


Fig.9 – Average bond-stress/bar slip curves plotted in a dimensionless form: (a) high-performance concrete; and (b) normal-strength concrete.

other hand, it is worth noting that the value 26 MPa (NSC) is reasonably close to those obtained in Bazant's tests ( $\sigma_0 = 22.8-28.8$  MPa, slightly-rusty bars, see Fig.2b), which are characterized by a more limited scattering among the different sets of specimens ( $\Delta\sigma_0 = \pm 12-13$  % with respect to the average value).

Eq. 1 can be very easily reformulated in a linear form:

$$f_c^2 / (\sigma_N - \sigma_0)^2 = A d_b + C \quad (2)$$

Once the points  $[f_c^2 / (\sigma_N - \sigma_0)^2, d_b]$  representing as many tests have been put in the reference plane (Fig.10), it is possible to perform the linear regressions for the two mixes. Once the vertical intercepts  $C$  and the slopes  $A$  have been worked out, the parameters  $B (= C^{-1/2})$  and  $d_0 (= C/A = A^{-1} B^{-2})$  can be evaluated. By introducing  $B$  and  $d_0$  into Eq.1, and by reverting to double-log scales for each test (Fig.11), it is possible to recognize that in the case of HPC the size effect law seems to describe well the transition from the strength criterion to linearly-elastic fracture mechanics (Fig.11a). In the case of NSC (Fig.11b) Eq.1 does not work, even if there is a sort of transition towards linear fracture mechanics, for the largest diameter. One possible explanation may be that in the weaker concrete bar roughness tends to produce more in-depth damage, than in the stronger concrete.

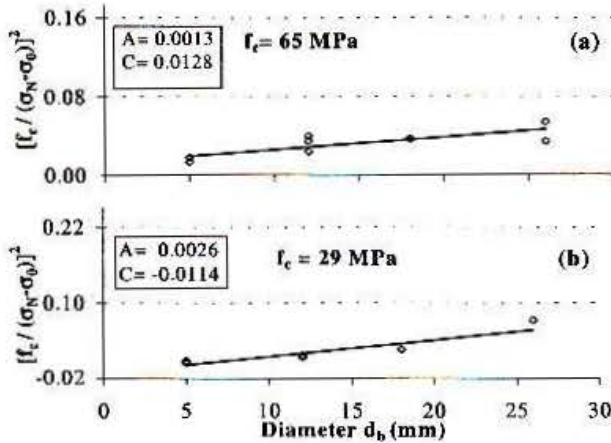


Fig.10 – Linear regressions of test data according to size-effect law: (a) HPC; and (b) NSC.

Consequently, in the former case the damage is no longer localized at the interface, making interface softening mixed with material microcracking. In the end, the anchorage behavior tends to be less size-sensitive.

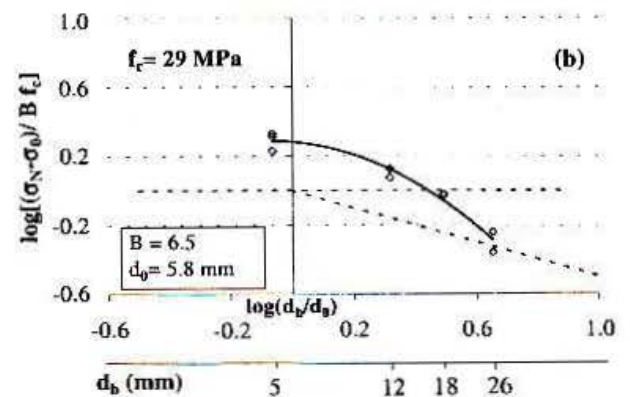
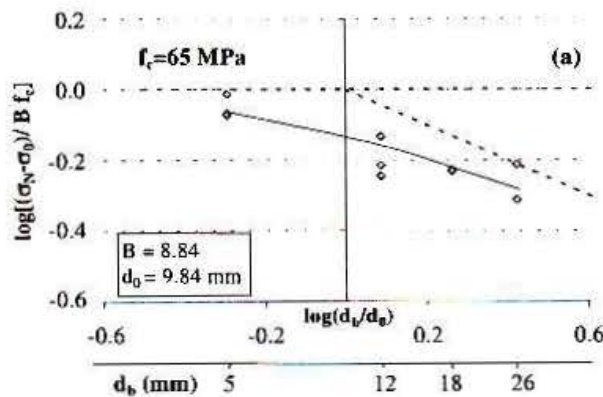


Fig.11 – Summary of the test results in double-logarithmic scales (19 tests out of 24), and their optimum fit by size-effect law: (a) high-performance concrete; and (b) normal-strength concrete.

## 6 DEBONDED LENGTH AND DEBONDING ENERGY

As well known, some parameters concerning bond can hardly be measured directly. The debonded length at any given load and the debonding energy (i.e. the energy required to increase the debonded interface by a unit value) can be cited, as well as bond stiffness.

In order to evaluate the above-mentioned parameters with reference to the two mixes used in this project, the approach introduced by Stang et al. (1990, modelling of pull-out) and later applied to smooth bars by Li et al. (1998) was adopted.

According to this approach, the problem of a smooth bar embedded in a concrete cylinder is reduced to one dimension (Fig.2a), with constant sections (bar and concrete); moreover, the concrete is assumed to be perfectly stiff, the steel is elastic and the interface is described by an elastic-fracturing-frictional law (Fig.12).

For a given anchorage and a given load level, the unknowns of the problem are: the slip at the interface "s(x)", the debonded length "a", the bond strength " $\tau_y$ ", the residual bond strength " $\tau_f$ " (frictional strength), the bond stiffness "k\*" or the shear stiffness of the interface " $\omega = (\pi k^*/E_s A_s)^{1/2}$ ", and the debonding energy " $\Gamma$ ". Of course,  $\tau_f$  and  $\Gamma$  are - by their very nature - independent of bar diameter.

Since it is beyond the scope of this paper to go through all the details of Stang's approach and Li's developments, only a few basic aspects will be recalled in the following:

- bond equation:  $E_s A_s \frac{d^2 s}{dx^2} - \pi d_b \tau(s) = 0$  (3)
- boundary cond.:  $s'(0) = 0$ ;  $s'(L) = P/E_s A_s$  (4)
- continuity conditions:  $s(L-a)^+ = s(L-a)^-$   
 $s'(L-a)^+ = s'(L-a)^-$
- $\tau = k^* s/d_b$  for  $0 \leq x \leq L-a$ ;  $\tau = \tau_f$  for  $L-a < x \leq L$  (5)
- strength criterion:  $\tau_y = F(\tau_f, k^*, a')$ ,  $a' = a(P_{max})$  (6')
- energy criterion:  $\Gamma = F(P_{max}, a', k^*, \tau_f)$  (6'')

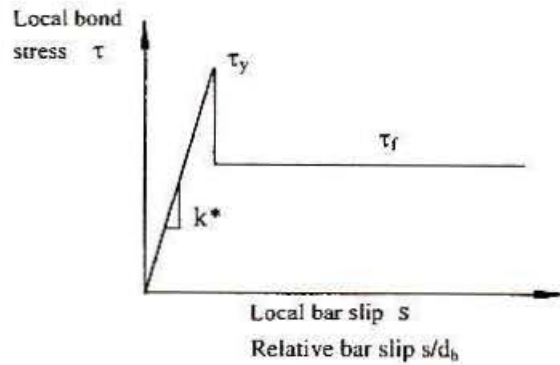


Fig.12 - Constitutive simplified local bond-stress/slip law.

Since  $P_{max}$ ,  $s(P_{max})$ ,  $dP/ds$  ( $a=0$ ) and  $\tau_f$  are known from the tests ( $\tau_f$  is here given the mean value of the bond-stress in the descending branches of the load-slip curves = 8.2 MPa, Fig.14), the integral of Eq.3 and the Eqs.4-6 are a system whose iterative solution makes it possible to work out all the unknown parameters.

In Figs.13a,b the applied load and the average bond stress are plotted as a function of the debonded length. In spite of the simplicity of the model, the plots of Fig.13 confirm that the capacity of the anchorage is reached in a state of advanced debonding, as indicated by the slip at the unloaded end (Fig.7). Furthermore, Fig.14 shows that  $\tau_y$  is strongly size-dependent, as should be in this approach, while  $\tau_f$  is a material property (size independent). Finally, the mean value of the debonding energy  $\Gamma$  turned out to be close to 600 J/m<sup>2</sup>, that is a few times larger than the fracture energy in tension of many silica-fume concretes (150-200 J/m<sup>2</sup>). Albeit partly ensuing from bar artificial roughness, these large values are not unexpected, since debonding is a sort of Mode-II fracture, which dissipates much more energy than Mode I.

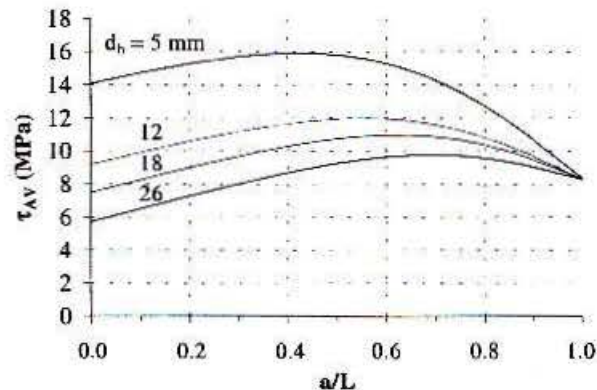
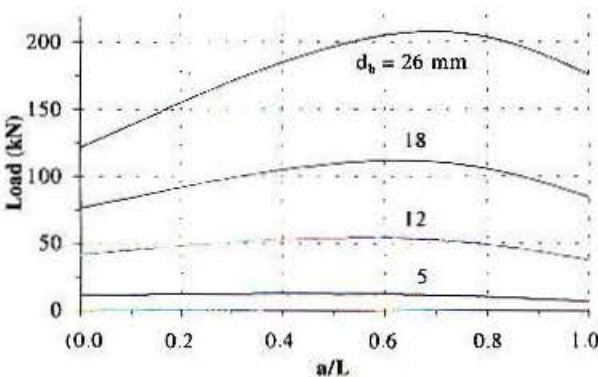


Fig.13 - High-performance concrete: plots of the applied load (a), and of the average bond stress (b), as a function of the debonded length, for different bar diameters.

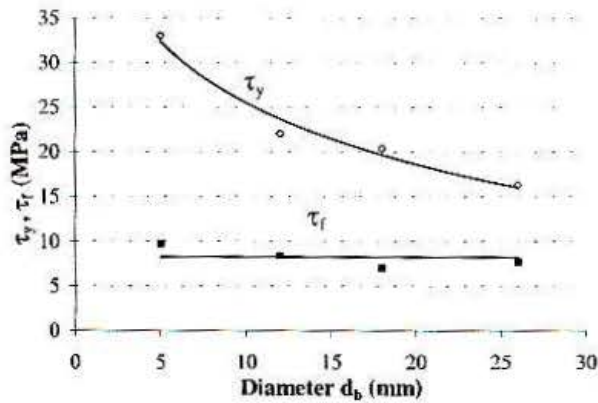


Fig.14 – Plots of the nominal and residual bond strengths as a function of bar diameter.

## 7 CONCLUDING REMARKS AND OUTLOOK

In spite of the well-founded theoretical reasons, which justify size effects in bar-concrete bond, the experimental evidence is still mixed and often disappointing, mainly because of the scattering of the test results, as confirmed also by the tests performed in this project (ordinary concrete).

However, the comparison between a high-performance concrete and an ordinary concrete shows clearly that bond is more size-dependent in the former, being also in good agreement with the well-known size-effect power law. The reasons are to be found in the lesser toughness and greater homogeneity of HPC.

Furthermore, this study shows that the frictional strength of bond is definitely greater in HPC, and that the debonding energy can be a few times larger than the fracture energy in tension (but it depends on how bond is modelled, since energy is a non-directly measurable parameter).

Finally, the proposed continuation of this project, and possibly of other similar projects, concerning both smooth and deformed bars, will contribute to ascertain the relevance of size effects, with respect to other, well-known aspects of bond. It is an intriguing theme, for both conceptual and practical reasons.

## ACKNOWLEDGMENTS

The authors are grateful to the Italian Ministry of the University and Research – MURST for funding of this work through the National Cooperative Research Project “Mechanical Deterioration and Durability of Normal and High-Performance Concrete Structures” (2000-2002). The tests were carried out by the third author in partial fulfillment of his MS degree requirements.

## REFERENCES

- Bazant, Z.P. and Chen, E.P. 1997. Scaling of structural failure. *Appl. Mech. Review* 50(10): 593-627.
- Bazant, Z.P. and Desmorat, R. 1994. Size effect in fiber or bar pull-out with interface softening slip. *ASCE - J. of Engrg. Mech.* 120(9): 1945-1962.
- Bazant, Z.P., Li, Z. and Thoma, M. 1995. Identification of stress-slip law for bar or fiber pullout by size effect tests. *ASCE - J. of Engrg. Mech.* 121(5): 620-625.
- de Larrard, F., Schaller, I. and Fuchs, J. 1993. Effect of bar diameter on the bond strength of passive reinforcement in HPC. *ACI - Mat. J.* 90(4): 333-339.
- Elfgrén, L., Noghabai, K., Ohlsson, U. and Olofsson, T. 1995. Application of fracture mechanics to anchors and bond. *Proc. 2<sup>nd</sup> Int. Conf. on Fracture Mech. of Concrete Struc. (FRAMCOS-2), Zurich (CH), Ed. by F. Wittmann, Publ. by AEDIFICATIO (Stuttgart, D): 1685-1694.*
- Esfahani, M.R. and Rangan, B.V. 1998. Local bond strength of reinforcing bars in normal-strength and high-strength concrete (HSC). *ACI-Struc. J.* 95(2): 96-106.
- Gambarova, P.G., Plizzari, G., Rosati, G.P. and Russo, G. (principal authors) 2000. Bond mechanics including pull-out and splitting failures, *Chapter 1 of FIB State-of-Art Report on “Bond of Reinforcement in Concrete” (Bulletin No.10), Ed. by R. Tepfers, Publ. by FIB: 1-98.*
- Li, Z., Xu, M. and Chui, N.C. 1998. Enhancement of rebar (smooth surface)-concrete bond properties by matrix modification and surface coatings. *Magazine of Concrete Research* 50(1): 49-57.
- Lorrain, M. and Hamouine, A. 1996. Bond performance of high-strength concrete. *Proc. of 4<sup>th</sup> Int. Symp. on the Utilization of HSC/HPC, Ed. by F. de Larrard and R. Lacroix, Publ. by LCPC, Paris (France): 1195-1200.*
- Morita, S., Fujii, S. and Kondo, G. 1994. Experimental study on size effect in concrete structures. *Size Effect in Concrete Structures, Ed. by H. Mihashi, H. Okamura and Z.P. Bazant, Publ. by E & FN Spon (London): 27-46.*
- Ozbolt, J. and Eligehausen R. 1996. Size effect in concrete and R/C structures – Diagonal shear and torsion. *Studi e Ricerche v.17, Politecnico di Milano (Milan, Italy): 37-68.*
- Park, R. and Paulay, T. 1975. Reinforced Concrete Structures. *John Wiley & Sons, New York.*
- Ravazzani, P. 2001. Size effects in bond: high-performance concrete versus normal-strength concrete (in Italian). *MS Thesis, Politecnico di Milano (Milan, Italy): 177 pp.*
- Sener, S. and Bazant, Z.P. 1994. Size effect in failure of bond splices of steel bars in R.C. beams. *Private Comm.: 17 pp.*
- Shah, S.P. and Ouyang, C. 1994. Fracture mechanics for failure of concrete. *Annu. Rev. Mater. Sci.* 24: 293-320.
- Soroushian, P. and Choi, K.B. 1989. Local bond of deformed bars with different diameters in confined concrete. *ACI - Structural J.* 86(2): 217-222.
- Stang, H., Li, Z. and Shah, S.P. 1990. Pull-out problem: stress versus fracture mechanical approach. *ASCE - J. of Engrg. Mech.* 116(10): 2136-2150.
- Yerlici, V.A. and Ozturan, T. 2000. Factors affecting anchorage bond strength in high-performance concrete. *ACI - Structural J.* 97(3): 499-507.